Acta Cryst. (1996). D**52**, 571–576

Crystallization and preliminary crystallographic analysis of *endo*-1,4-β-xylanase I from *Aspergillus niger*

UTE KRENGEL, HENRIËTTE J. ROZEBOOM, KOR H. KALK AND BAUKE W. DIJKSTRA *at BIOSON Research Institute and Laboratory of Biophysical Chemistry, Department of Chemistry, University of Groningen, Nijenborgh 4, 9747 AG Groningen, The Netherlands*

(*Received 28 August 1995; accepted 26 October 1995*)

Abstract

A family G xylanase from *Aspergillus niger* has been crystallized using the vapor-diffusion method. Several crystal forms could be obtained using various sodium salts as precipitants. Three of the crystal forms belong to space groups $P2_1$, $P2_12_12_1$ and $P4_3$ and have cell parameters of approximately $a = b = 85.1$, $c = 113.6$ Å and $\alpha = \beta = \gamma = 90°$. These crystal forms can be converted into one another by flash freezing or macroseeding. A fourth crystal form is cubic (space group $P2_13$) with unit-cell axes of $a = b = c = 112.3$ Å. Data sets for three of the four crystal forms have been collected, extending to a maximum resolution of 2.4 Å. The structures of the monoclinic and orthorhombic crystals have been solved by molecular replacement by combining the crystallographic information of the different crystal forms. Refinement of the orthorhombic crystal form is now in progress.

1. Introduction

Xylanases (Visser, Beldman, Kusters-van Someren & Voragen, 1992) belong to the glycanase enzyme family and are characterized by their ability to degrade xylan yielding short-chain xylo-oligosaccharides. Several xylanase subclasses exist, like *endo-* and *exo-*, 1,4- and 1,3-enzymes, which differ in molecular weight, pH optimum and substrate specificity. All these enzymes can be grouped into two families, F and G, based on hydrophobic cluster analysis and sequence homology (Gilkes, Henrissat, Kilburn, Miller & Warren, 1991). Families F and G correspond to families 10 and 11 in the numerical classification of glycosyl hydrolases (Henrissat, 1991; Henrissat & Bairoch, 1993).

Since xylanases play a crucial role in the breakdown of plant cell walls and cell-wall constituents (xylan is the most abundant hemicellulose), they are of major importance for a large number of industrial applications ranging from the clearing of fruit juices to benefits in paper industry. In food industry, xylanase-supplemented food plays an important role in effective feeding and reduction of animal excrements. Especially fungal xylanases, which generally have lower pH optima, are ideally suited to release important nutrients in such acidic environments as the animal stomachs. The enzyme we are working with is produced at industrial scale by the company Gist-Brocades (van den Broeck *et al.*, 1992). It is used as a supplement in chicken food.

A major goal of our research is to improve the properties of the *A. niger* xylanase by protein engineering. For this, we need to establish the catalytic mechanism under low-pH conditions, which is only possible with the knowledge of the three-dimensional structure of the enzyme. Although already several structures of family G xylanases have been published (Campbell *et al.*, 1993; Wakarchuk, Campbell, Sung, Davoodi & Yaguchi, 1994; Törrönen, Harkki & Rouvinen, 1994; Törrönen & Rouvinen, 1995), they do not seem to be suitable as a basis for the protein-engineering studies envisaged, because of the relatively low sequence identity of *ca* 45%. Even xylanase I from *Trichoderma reesei* (Törrönen *et al.*, 1992), which has a similarly low pH optimum as the *Aspergillus niger* xylanase I, is only 53% identical.

2. Experimental

2.1. *Purification and crystallization*

The *endo*-1,4-β-xylanase I (E.C. 3.2.1.8) from *Aspergillus niger* is available as a powder from the company Gist-Brocades in Delft, The Netherlands. In addition to the recombinant xylanase enzyme, this powder contains one other protein and a significant amount of salt.

1 g of the powder was suspended in 6 ml 50 m*M* sodium acetate buffer (pH 4.7) and centrifuged to remove the residual precipitant. The supernatant was desalted using a PD-10 column (Pharmacia) and subsequently loaded on a Superdex 75 fast protein liquid chromatography (FPLC) column (Pharmacia). After gel filtration, the two proteins were clearly separated as determined by UV absorption measurements. A specific β-xylanase activity test using XYLAZYME tablets (Megazyme) confirmed that the xylanase eluted from the column as the second peak.

For crystallization, the protein was buffered in 10 m*M* sodium acetate, pH 4.7, and concentrated in a Filtron-10K macroconcentrator tube to a final concentration of 4.5 mg ml^{-1}.

Crystallization conditions were explored at 295, 277 and 310 K, using the hanging-drop and sitting-drop vapor-diffusion methods as well as the batch method. Various precipitants, additives and pH's were tested (*e.g.* using the matrix-96; Sarfaty & Hol, personal communication), and several seeding techniques (micro, macro, streak seeding) were applied.

2.2. *X-ray diffraction experiments*

X-ray diffraction data were either collected at room temperature from crystals mounted in thin-walled glass capillaries (Glass W. Müller) or at 120 K after flash freezing the crystals using appropriate stabilizing solutions and loops made from rayon fibers or dental floss. As a cryoprotectant, ethylene glycol proved most effective. 20% of this reagent were included in the respective mother liquors. In addition, it turned out to be essential to add protein to the stabilizing solutions in order to prevent the crystals from deteriorating. However, the protein did not necessarily have to be xylanase; other proteins like *e.g.* bovine serum albumin were equally usable. Because of solubility problems, the stabilizing solutions were prepared using vapor-diffusion techniques like those used in sitting-drop

crystallization experiments. For this, a drop of protein solution was mixed with an equal volume of a reservoir solution containing the normal mother liquor plus cryoprotectant.

X-ray diffraction data were collected in house using an Enraf–Nonius FAST area-detector system or at the EMBL outstation at DESY, at beamlines X31, X11 or BW7B which are equipped with MAR image plates.

The FAST data were collected and processed using the program suite *MADNES* (Messerschmidt & Pflugrath, 1987) and scaled with the programs *SELDAT*, *SCALKB*2 and *KBAPLY* from the *BIOMOL* package (*BIOMOL* software, Crystallographic Computing Package, Protein Crystallography Group, University of Groningen, The Netherlands). The synchrotron data were reduced with *XDS* (Kabsch, 1988*a*,*b*, 1993) or *DENZO* and *SCALEPACK* (Otwinowski, 1993) and intensities converted to structure-factor amplitudes ($|F|$) with the program *TRUNCATE* from the *CCP*4 suite (Collaborative Computational Project, Number 4, 1994), using the option *TRUNCATE NO*. With this setting, the program *TRUNCATE* merely converts intensities to $|F|$'s without applying any truncation procedure. Application of the truncation procedure according to French & Wilson (1978) was avoided, because it can cause serious damage to the weak data if the data have already been modified in a previous analysis step.

2.3. *Self-rotation and self-Patterson analysis*

Self-rotation and self-Patterson functions were both calculated at 8–3.0 Å resolution, using the programs *FROTF*0-3 and *FSFOR* from the Groningen *BIOMOL* package, respectively. Maps were calculated in 2.5° steps for the Eulerian angles α and γ and in 5° steps for the angle β for the self-rotation searches and in 0.9 Å steps in self-Patterson analysis.

2.4. *Molecular replacement*

The coordinates of a family G xylanase from *Trichoderma harzianum* were kindly provided by Dr D. R. Rose (Campbell *et al.*, 1993) and served as a search model for molecular-replacement analysis. In the meantime, the coordinates of this structure have been deposited at the Brookhaven Protein Data Bank (ID code 1XND). The two xylanases of *T. harzianum* and *A. niger* have 45% sequence identity.

Rotation searches were carried out using the programs *FROTF*0-3 and from the Groningen *BIOMOL* package which are based on Crowther's fast-rotation function (Crowther, 1972). All the calculations were carried out in parallel for two resolution ranges of 10–3.0 and 8–3.5 Å. The radius of integration for the Patterson sphere was chosen to be six times the high-resolution value, thus 18 and 21 Å, respectively. These values correspond approximately to the radius of the model structure. The model in its PDB orientation was placed into an orthogonal unit cell with *P*1 symmetry, for which the cell axes were chosen to be slightly larger than the sum of molecule diameter and integration radius. Maps were calculated in 2.5° steps for the Eulerian angle α and in 5° steps for the angles β and γ, respectively.

Subsequently, the correctly oriented molecules were positioned in the crystal unit cell using the *BIOMOL* program *TRAFUN*, which is based on the Crowther and Blow translation function (Crowther & Blow, 1967), and the program *BRUTE* (Fujinaga & Read, 1987), a six-dimensional correlation coefficient targeted search program. For both translation searches, three resolution ranges were tested, 10–0.04, 10–0.03 and 8–3.5 Å, of which the first resolution range proved to give the sharpest peaks. Maps were calculated with grid spacings of 1–2 Å where necessary.

The final solutions were visually verified by inspecting the molecular packing on a graphics workstation using *O* (Jones, Zou, Cowan & Kjeldgaard, 1991) and subsequently subjected to rigid-body refinement as implemented in *X-PLOR* (Brünger, Kuriyan & Karplus, 1987; Brünger, 1993).

3. Results and discussion

3.1. *Crystal analysis*

Most of the screened crystallization conditions yielded either no crystals at all or highly twinned crystals. However, relatively high numbers of non-twinned crystals could be obtained using sodium sulfite, sodium thiosulfate or sodium sulfate as precipitants (see Table 1 and Fig. 1). Best results were achieved at 295 K applying the hanging-drop method (or sitting drops on siliconized glass wells) and macroseeding techniques. Interestingly, crystals were found to change cell parameters upon seeding into a different mother liquor.

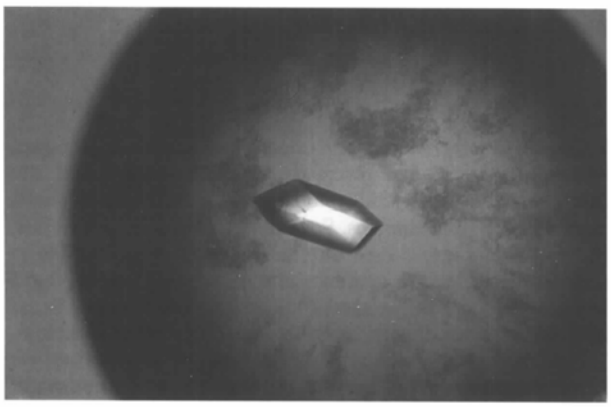

(*a*)

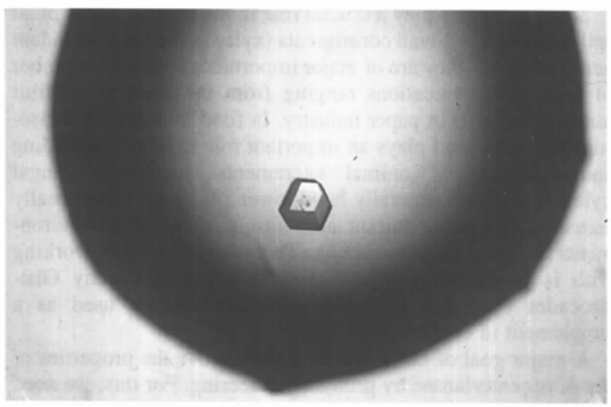

(*b*)

Fig. 1. (*a*) Monoclinic crystal form. Approximate crystal dimensions are 0.25 × 0.25 × 0.56 mm. The shape of this crystal is also typical for the orthorhombic and tetragonal xylanase crystals. (*b*) Cubic crystal form. Dimensions of this crystal are 0.20 × 0.20 × 0.20 mm.

Table 1. *Crystallization conditions and crystal parameters*

Drop	2 µl 4.5 mg ml^{-1} xylanase in 10 m*M* $NaCH_3COOH$, (pH 4.7) mixed with 2 µl of the respective reservoir solutions
Reservoir 1	1.55 *M* Na_2SO_3 (pH 9.0) 1% *n*-propanol or 2.5 m*M* EDTA
Remarks	Best results if macroseeded into drops without additives.
Space group	$P2_1$
Cell parameters (Å, °)	$a = 84.5$ $b = 113.5$ $c = 85.6$ $\beta = 92.4$
Reservoir 2	1.8–1.85 *M* $Na_2S_2O_3$ (pH 8.0) with or without addition of 1% *n*-propanol
Remarks	The yield of perfect crystals greatly increased when macroseeded into drops including 1% *n*-propanol.
Space group	$P2_12_12_1$
Cell parameters (Å)	$a = 84.3$ $b = 85.3$ $c = 113.8$
Reservoir 3	0.65–1 *M* Na_2SO_4 50 m*M* Borax/KH_2PO_4 1:1, (pH 8.9) either no additives or 1% *n*-propanol or 1% ethanol
Remarks	Macroseeding techniques greatly improved the results.
Space groups and cell parameters (Å)	$P4_3$* $a = b = 85.1$ $c = 113.6$ $P2_12_12_1$ $a = 84.3$ $b = 85.3$ $c = 113.8$
Reservoir 4	1.85–2 *M* $NaHSO_3/Na_2SO_3$ 1:1 (pH 6.3)
Remarks	No birefringence, low reproducibility.
Space group	$P2_13$
Cell parameters (Å)	$a = b = c = 112.3$

* For the tetragonal crystal form, no complete data set was available. The space group was therefore deduced only indirectly, from the cell parameters, the similarity to the monoclinic and orthorhombic crystal forms (as demonstrated by seeding and flash-freezing experiments) and from crystal packing of those two crystal forms (as determined by molecular replacement).

Macroseeds typically grew to a size of 0.2 × 0.2 × 0.5 mm within several weeks. Only the cubic crystals grew to large sizes (0.4 × 0.4 × 0.4 mm) without applying seeding techniques. However, these crystals sometimes took several months or a year to appear and were thus difficult to reproduce. Furthermore, this crystal form turned out to be very sensitive to X-irradiation and had rather poor diffraction quality.

The space group for these crystals was determined to be $P2_13$ with unit-cell axes of $a = b = c = 112.3$ Å. From this, the Matthews parameter was calculated to be 2.95 Å^3 Da^{-1} assuming two molecules per asymmetric unit ($M_r = 20$ kDa). This corresponds to a relatively high solvent content of 58.3% (Matthews, 1968). Upon flash freezing, the cell axes shrink to $a = b = c = 109.6$ Å.

All the other crystal forms have cell parameters close to $a = b = 85.1$, $c = 113.6$ Å and $\alpha = \beta = \gamma = 90°$ (see Table 1). The corresponding Matthews parameter is 2.57 Å^3 Da^{-1} assuming eight molecules per asymmetric unit for the monoclinic crystals ($P2_1$) and four molecules in the asymmetric unit for the orthorhombic ($P2_12_12_1$) and tetragonal crystal forms ($P4_3$). This corresponds to a solvent content of *ca* 52.1%.

Also for these crystals, cell shrinkage was found to occur upon flash freezing. In addition, another very interesting phenomenon was observed. While tetragonal crystals were rather stable when subjected to cryogenic temperatures, monoclinic and orthorhombic crystals often switched to the higher symmetry space groups when shock frozen. These observations together with the changing of cell parameters during macroseeding strongly suggested very similar crystal packing in the different crystal forms and the existence of a non-crystallographic fourfold axis in the monoclinic and orthorhombic crystal forms.

3.2. *Diffraction data*

For three of the four crystal forms, complete data sets have been obtained. Initially, diffraction data were collected in house at room temperature using a rotating copper anode as X-ray source. A 3.0 Å data set with an $R_{merge}(I)$ of 6.6% was obtained for the monoclinic crystal form. The data set is 96.0% complete (91.2% in the last resolution shell from 3.2 to 3.0 Å), comprising 30 995 unique reflections with an average redundancy of 1.6.

For the orthorhombic crystal form, grown from sodium thiosulfate solutions, a 2.4 Å data set was collected at beamline X31 at the EMBL outstation of DESY, Hamburg ($\lambda = 0.99$ Å, $T \simeq 295$ K). In total, 33 131 unique reflections were recorded, corresponding to an overall completeness of 95.3% (94.8% for data in the resolution shell from 2.6 to 2.4 Å and 51.0% for data from 2.4 to 2.35 Å, respectively). The symmetry R factor for the intensities is 8.2% and the average redundancy of the data 4.6.

For the cubic crystals, two data sets were collected at the DESY beamlines BW7B ($\lambda = 0.87$ Å) and X11 ($\lambda = 0.93$ Å), one at room temperature and one at cryogenic temperature. At room temperature, the crystal decayed within 15 min and only an incomplete data set could be obtained covering 8.75° of the Ewald sphere. Due to the cubic symmetry, however, the data were nevertheless 64.8% complete to 3.0 Å resolution (50.7% from 3.2 to 3.0 Å), comprising 6393 unique reflections with an average redundancy of 1.4 [$R_{sym}(I) = 4.8\%$].

Even at cryogenic temperature, the cubic crystals, which initially diffracted to 2.8 Å resolution, slowly decayed. As a consequence, data were only used to 3.2 Å resolution [$R_{sym}(I) = 7.3\%$ for all data to 3.2 Å]. The data set was 99.7% complete after scanning 37.8° of the Ewald sphere, comprising 7456 of the theoretically predicted reflections with an average redundancy of 4.5.

In further analysis, the attention was focussed on the orthorhombic and monoclinic crystal forms due to the superiority of those diffraction data.

3.3. *Self-rotation analysis*

Self-rotation analysis confirmed the expectations concerning similar packing of the monoclinic, orthorhombic and tetragonal crystal forms. In both, the monoclinic and orthorhombic crystal forms, three twofold axes were found to be running approximately or exactly parallel to the cell axes, and a fourfold axis was found to be aligned with the axes corresponding to the c axis of the tetragonal crystals. The peak height for these non-crystallographic symmetry axes ranged between 84 and 88% of the crystallographic peak heights.

The results of the self-rotation searches are consistent with the existence of eight differently oriented molecules in the respective unit cells.

3.4. *Self-Patterson analysis*

Self-Patterson searches were carried out since the Matthews parameter pointed to 16 molecules occupying the respective unit cells of the monoclinic and orthorhombic crystal forms, while self-rotation analysis indicated that only eight different orientations existed. It thus seemed likely that the molecules can be grouped into eight pairs of two similarly oriented molecules which are related by translation.

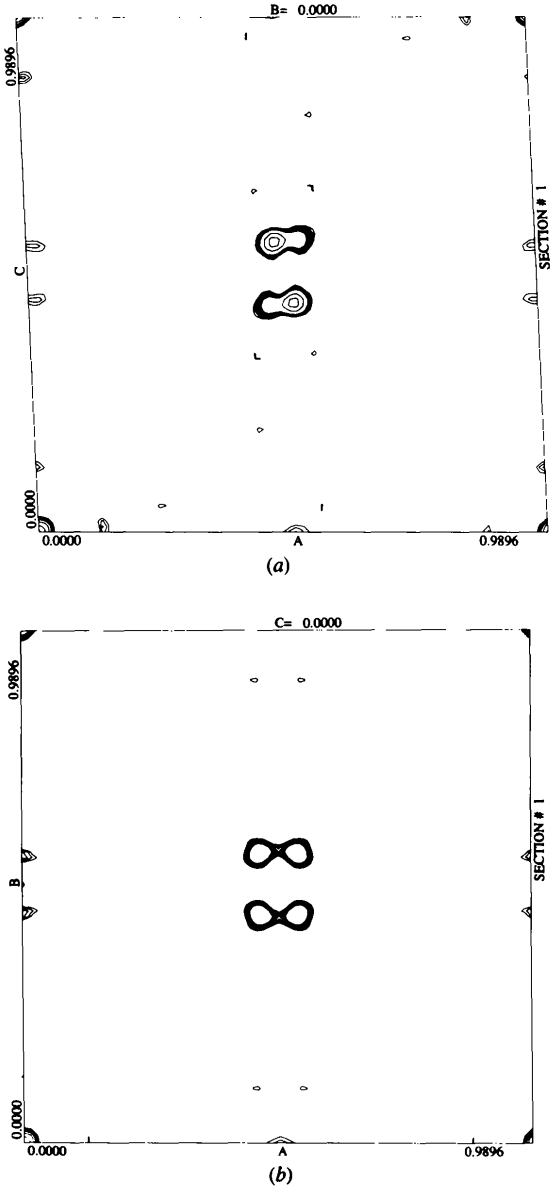

Fig. 2. Sections of the self-Patterson maps for (*a*) the monoclinic and (*b*) the orthorhombic crystal forms. Maximum peak heights are 63% of the origin peak height for the monoclinic crystal form and 6% for the orthorhombic crystal form. Note that the *c* axis of the orthorhombic crytals corresponds to the *b* axis of the monoclinic crystals.

For both the monoclinic and orthorhombic crystal forms, the self-Patterson function exhibited peaks at similar positions (see Fig. 2). In the case of the monoclinic crystals, however, the peaks were rather high, with peak heights of 63% of the origin value. They were found at $u_1 = 0.52$, $w_1 = 0.44$ and its inverse $-u_1 = 0.48$, $-w_1 = 0.56$ and were smeared out along u, having a minor second maximum (27% of the origin peak height) at $u_2 = 0.47$, $w_2 = 0.44$. For the orthorhombic crystal form on the other hand, four peaks with equal, but low peak heights (6% of the origin value) were found at positions corresponding to $u_1 = 0.54$, $w_1 = 0.44$ and $u_2 = 0.46$, $w_2 = 0.44$ of the monoclinic crystal form and the respective inverse positions. The peak heights were somewhat higher (10%) when only lower resolution data were considered (high-resolution cut-off at 4 Å instead of 3 Å).

The results of the self-Patterson analysis indicates that molecules are indeed pairwise related by self-Patterson vectors and that for the orthorhombic crystals the orientations of the respective paired molecules are not absolutely identical.

3.5. *Molecular replacement*

Cross-rotation searches lead to similar results for the monoclinic and orthorhombic crystal forms. In either case, the molecules in the asymmetric unit were found to adopt four different orientations which were related to each other by the non-crystallographic symmetry operators determined by self-rotation analysis. The four orientations were determined by rotating the unmodified *T. harzianum* model structure by Eulerian angles $[\alpha, \beta, \gamma]_1 = [140$ or $138, 60, 315°]$, $[\alpha, \beta, \gamma]_2 = [42.5$ or $43, 120, 135°]$, $[\alpha, \beta, \gamma]_3 = [50$ or $49, 60, 315°]$ and $[\alpha, \beta, \gamma]_4 = [128.5$ or $131.5, 120, 135°]$ for the monoclinic and orthorhombic crystal forms, respectively. These solutions corresponded to the four highest peaks of the cross-rotation functions. For both crystal forms, the correct peaks were less than 1σ above the highest noise peak.

Translation analysis turned out to be more difficult than expected. For the orthorhombic crystal form, it even was impossible to determine the positions of the molecules using the programs *TRAFUN* and *BRUTE* in the conventional way. For the monoclinic crystal form, three strong consistent peaks were found in translation searches with *TRAFUN*, corresponding to one peak each for three of the four different orientations. The next highest peaks had a peak height of 59, 87 and 70% compared to the highest peak of the respective orientations. Since the results of self-Patterson analysis suggested the existence of two peaks per orientation, the peak lists were screened for a second peak which would be related to the highest translation peak by the self-Patterson vector, however without success. In the course of further analysis, it turned out that the highest peaks for the three respective orientations indeed corresponded to the correct solutions. Only the interpretation of the peaks was initially wrong. In the output of the program *TRAFUN*, peaks represent difference vectors between molecules of two different asymmetric units. From these, the position of the molecules in the cell can be calculated. In the special situation where two molecules in an asymmetric unit have the same orientation, three possible difference vectors exist (see Fig. 3): two of them relate the molecules in the asymmetric unit to their crystallographic counterparts (1–4, 2–3), the third vector relates the molecules to the self-Patterson mates of the crystallographically related molecules (1–3, 2–4). Since there are two possibilities to satisfy the latter relation, this

third peak should be twice as high as the other two peaks. With this knowledge, the positions of six of the eight molecules occupying the asymmetric unit of the monoclinic crystal form were easily determined. The solutions were verified by translation analysis of an artificially created dimer (of which the monomers were related by the self-Patterson vector). For the fourth orientation, the translation function was too noisy to determine the positions of the respective molecules.

In a second step, the program *BRUTE* was used to determine the positions of the two missing molecules and to relate all molecules with respect to a common origin. Upon positioning the eight molecules in the asymmetric unit, the real-space correlation coefficient increased from 10.6 to 38.1% and the R factor dropped from 54.6 to 46.9%. The final positions as determined by molecular replacement are given in Table 2(*a*).

For the orthorhombic crystal form, the translation problem could not be solved in the conventional way. To overcome this problem, we re-indexed the orthorhombic data in the monoclinic space group $P2_1$ and repeated molecular replacement. The results of both cross-rotation and translation analysis were found to be very similar to the 'real' monoclinic solutions. Therefore, the correct positions of the original monoclinic analysis were immediately refined with the program *BRUTE*. The final solutions for the orthorhombic crystal form are given in Table 2(*b*). The corresponding correlation coefficient and R factor are 34.2 and 52.6%, respectively.

3.6. *Verification of molecular-replacement results*

Molecular packing was verified by visual inspection on the graphics screen, as well as by comparing the molecular replacement solutions with the results from self-rotation and self-Patterson analysis.

Since no clashes between molecules were observed, crystal packing in principle seemed possible. Furthermore, the molecules were found to be arranged around fourfold screw axes as was expected since self-rotation searches had revealed a fourfold symmetry axis to be aligned parallel to a crystallographic twofold screw axis. The identification of this screw axis is consistent with the assignment of the tetragonal space group as being $P4_3$.

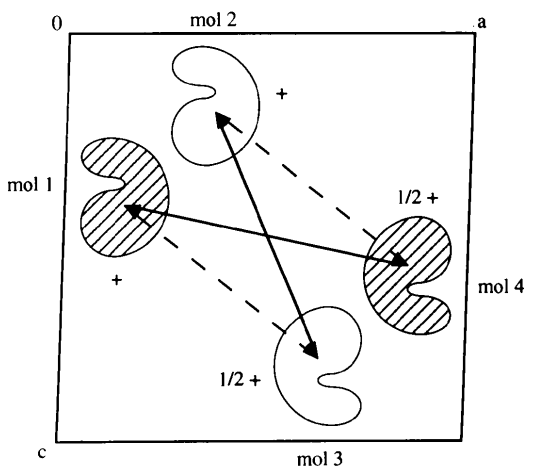

Fig. 3. Sketch of a unit cell with $P2_1$ symmetry which contains two molecules of equal orientation in the same asymmetric unit. Solid arrows indicate difference vectors between crystallographically related molecules, dashed arrows difference vectors between a molecule and the self-Patterson mate of its crystallographic counterpart.

Table 2. *Translation solutions for the monoclinic and orthorhombic crystal forms*

	(*a*) Translation solutions for the monoclinic crystal form			(*b*) Translation solutions for the orthorhombic crystal form		
	x	y	z	x	y	z
rot1/trans1	0.36	0.10	0.23	0.36	0.10	0.23
trans2	0.88	0.11	0.67	0.89	0.11	0.67
rot2/trans1	0.39	0.25	0.84	0.39	0.25	0.83
trans2	0.86	0.25	0.27	0.85	0.25	0.27
rot3/trans1	0.30	0.37	0.39	0.29	0.36	0.40
trans2	0.82	0.36	0.85	0.82	0.35	0.84
rot4/trans1	0.30	0.00	0.54	0.32	0.00	0.65
trans2	0.79	0.00	0.11	0.78	0.00	0.10

Notes: translation solutions for the orthorhombic crystal form are given as determined by molecular replacement using the orthorhombic crystal data re-evaluated in space group $P2_1$. The so obtained positions were converted to the correct positions in the orthorhombic cell ($x_{ortho} = x + 0.25$, $y_{ortho} = -z$, $z_{ortho} = y + 0.82$) prior to rigid-body refinement. Note that the translation of 0.82 along the monoclinic b axis relates the orthorhombic origin to the arbitrarily chosen monoclinic origin.

Also, the different patterns of the self-Patterson maps could now be explained: while in the monoclinic crystals, three of the four molecule pairs were related to each other by only one difference vector (or its inverse), the orthorhombic crystals contained two times two pairs of molecules related by different self-Patterson vectors (as can easily be seen from Table 2). These two vectors had the same w component, but inverse u components, so that together with their respective inverses, four peaks could be found in the self-Patterson map, which were arranged symmetrically around $u = 0.5, w = 0.5$. In the self-patterson map of the orthorhombic crystals, the peaks were rather sharp, but low, while the two major peaks in the monoclinic map had a peak height of two thirds of the origin peak, but were smeared out significantly along u, showing a lower second maximum at a position similar to the additional peak in the self-Patterson map of the orthorhombic crystal form. The differences in peak heights in the two self-Patterson maps have two different causes. First, the ratio of molecule pairs related by the one or other self-Patterson vector is different for the two crystal forms (3:1 for the monoclinic and 2:2 for the orthorhombic crystals). Second, the paired molecules in the monoclinic crystals have almost identical orientations, while the orientations of the self-Patterson mates in the orthorhombic crystals differ in average by 10° (as determined after rigid-body refinement). These differences in orientation probably also account for the encountered difficulties with molecular replacement for the orthorhombic crystal form. In summary, the molecular-replacement solutions are found to be consistent with the results from both self-rotation and self-Patterson analysis.

The structure of the orthorhombic crystal form is currently being refined and will be published elsewhere.

We would very much like to thank the people at the company Gist-Brocades and especially Dr Jan Metske van der Laan for a very fruitful collaboration. Furthermore, we are very grateful to Dr David Rose who made the coordinates of the *T. harzianum*

xylanase available to us. Without his support, this work could not have been completed within such a short period of time. And last, but not least, we would like to thank the staff at the EMBL Hamburg Outstation, c/o DESY for their kind support during data collection, and the European Union for financial support of the work at EMBL Hamburg through the HCMP to Large Installations Project, contract No. CHGE-CT93-0040.

References

Broeck, H. C. van den, de Graaff, L. H., Hille, J. D. R., van Ooyen, A. J., Visser, J. & Harder, A. (1992). Eur. Patent Application EPA 0463706A1, Gist-Brocades.

Brünger, A. T. (1993). *X-PLOR. Version 3.1. A System for Crystallography and NMR.* Yale University, New Haven, CT, USA.

Brünger, A. T., Kuriyan, J. & Karplus, M. (1987). *Science*, **235**, 458–460.

Campbell, R. L., Rose, D. R., Wakarchuk, W. W., To, R., Sung, W. & Yaguchi, M. (1993). *Proceedings of the Second TRICEL Symposium on Trichoderma reesei Cellulases and other Hydrolases*, Espoo, Finland, 1993, edited by P. Suominen & T. Reinkainen, pp. 63–72. Helsinki: Foundation for Biotechnical and Industrial Fermentation Research.

Collaborative Computational Project, Number 4 (1994). *Acta Cryst.* D**50**, 760–763.

Crowther, R. A. (1972). *The Molecular Replacement Method*, edited by M. G. Rossmann, pp. 173–178. New York: Gordon and Breach.

Crowther, R.A. & Blow, D. M. (1967). *Acta Cryst.* **23**, 544–548.

French, S. & Wilson, K. (1978). *Acta Cryst.* A**34**, 517–525.

Fujinaga, M. & Read, R. (1987). *J. Appl. Cryst.* **20**, 517–521.

Gilkes, N. R., Henrissat, B., Kilburn, D. G., Miller, R. C. & Warren, R. A. J. (1991). *Microbiol. Rev.* **55**, 303–315.

Henrissat, B. (1991). *Biochem. J.* **280**, 309–316.

Henrissat, B. & Bairoch, A. (1993). *Biochem. J.* **293**, 781–788.

Jones, T. A., Zou, J.-Y., Cowan, S. W. & Kjeldgaard, M. (1991). *Acta Cryst.* A**47**, 110–119.

Kabsch, W. (1988*a*). *J. Appl. Cryst* **21**, 67–71.

Kabsch, W. (1988*b*) *J. Appl. Cryst.* **21**, 916–924.

Kabsch, W. (1993). *J. Appl. Cryst.* **26**, 795–800.

Matthews, B. W. (1968). *J. Mol. Biol.* **33**, 491–497.

Messerschmidt, A. & Pflugrath, J. W. (1987). *J. Appl. Cryst.* **20**, 306–315.

Otwinowski, Z. (1993). *DENZO. An Oscillation Data Processing Suite for Macromolecular Crystallography.* Yale University, New Haven, CT, USA.

Sarfaty, S. & Hol, W. G. J. (1992). Personal communication.

Törrönen, A., Mach, R. L., Messner, R., Gonzalez, R., Kalkkinen, N., Harkki, A. & Kubicek, C. P. (1992). *BioTechnol.* **10**, 1461–1465.

Törrönen, A., Harkki, A. & Rouvinen, J. (1994). *EMBO J.* **13**, 2493–2501.

Törrönen, A. & Rouvinen, J. (1995). *Biochemistry*, **34**, 847–856.

Visser, J., Beldman, G., Kusters-van Someren, M. A. & Voragen, A. G. J. (1992). *Xylans and Xylanases. Progress in Biotechnology* Vol. 7. Amsterdam: Elsevier.

Wakarchuk, W. W., Campbell, R. L., Sung, W. L., Davoodi, J. & Yagachi, M. (1994). *Protein Sci.* **3**, 467–475.